

Supervised training of spiking neural networks for robust deployment on mixed-signal neuromorphic processors

Julian Büchel^{1,2}, Dmitry Zendrikov², Sergio Solinas³,
Giacomo Indiveri^{1,2}, Dylan R. Muir^{1,*}

Abstract

Mixed-signal analog/digital electronic circuits can emulate spiking neurons and synapses with extremely high energy efficiency, following an approach known as “neuromorphic engineering”.

However, analog circuits are sensitive to variation in fabrication among transistors in a chip (“device mismatch”). In the case of neuromorphic implementation of Spiking Neural Networks (SNNs), mismatch is expressed as differences in effective parameters between identically-configured neurons and synapses. Each fabricated chip therefore provides a different distribution of parameters such as time constants or synaptic weights.

Without the expensive overhead in terms of area and power of extra on-chip learning or calibration circuits, device mismatch and other noise sources represent a critical challenge for the deployment of pre-trained neural network chips.

Here we present a supervised learning approach that addresses this challenge by maximizing robustness to mismatch and other common sources of noise.

The proposed method trains SNNs to perform temporal classification tasks by mimicking a pre-trained dynamical system, using a local

¹SynSense, Thurgauerstrasse 40, 8050 Zurich, Switzerland; ²Institute of Neuroinformatics, University of Zurich and ETH Zurich, Winterthurerstrasse 190, 8057 Zurich, Switzerland; ³Department of Biomedical Science, University of Sassari, Piazza Università, 21, 07100 Sassari, Sardegna, Italy; *dylan.muir@synsense.ai

learning rule adapted from non-linear control theory. We demonstrate the functionality of our model on two tasks that require memory to perform successfully, and measure the robustness of our approach to several forms of noise and variability present in the network. We show that our approach is more robust than several common alternative approaches for training SNNs.

Our method provides a viable way to robustly deploy pre-trained networks on mixed-signal neuromorphic hardware, without requiring per-device training or calibration.

Dedicated hardware implementations of Spiking Neural Networks (SNNs) are an extremely energy-efficient computational substrate on which to perform signal processing and machine learning inference tasks.^{1–8} Optimal energy efficiency is achieved when using mixed-signal analog/digital neuron and synapse circuits following an approach known as “neuromorphic engineering”.⁹ In these hardware devices, large arrays of neurons and synapses are physically instantiated in silicon, and coupled with flexible digital routing and interfacing logic in “mixed-signal” designs.^{2,6}

However, all analog silicon circuits suffer from process variation across the surface of a chip, changing the operating characteristics of otherwise identical transistors — known as “device mismatch”.^{10,11} In the case of spiking neurons implemented using analog or mixed-signal circuits, mismatch is expressed as parameter variation between neurons and synapses that are otherwise configured identically.^{12–15} The parameter mismatch on each device appears as frozen parameter noise, introducing variance between neurons and synapses in time constants, thresholds, and weight strength.

Parameter noise in mixed-signal neuromorphic devices can be exploited as a symmetry-breaking mechanism, especially for neural network architectures that rely on randomness and stochasticity as a computational mechanism.^{16–19} However, random architectures can raise problems for commercial deployment of applications on mixed-signal devices: the parameter noise would affect neuronal response dynamics, and these device to device variations could affect and degrade the system performance of individual chips. A possible solution would be to perform a post-production device calibration step or re-training, but this would raise deployment costs

significantly and not scale well with large volumes. In addition to device mismatch, mixed-signal neuromorphic systems also suffer from other sources of noise, such as thermal noise or quantisation noise introduced by restricting synaptic weights to a low bit-depth.

In contrast to current mainstream Deep Neural Networks (DNNs), spiking networks suffer from a severe configurability problem. The backpropagation algorithm permits configuration of extremely deep NNs for arbitrary tasks,²⁰ and is effective also for network models with temporal state,²¹ but is difficult to apply to the discontinuous dynamics of SNNs.²²⁻²⁴ Methods to approximate the gradient calculations by using surrogate functions,²⁵ eligibility traces²⁶ or adjoint networks²⁷ have provided a way to adapt backpropagation for spiking networks. Non-local information is required for strict implementation of the backpropagation algorithm, but random feedback²⁸ and local losses²⁹ have been employed with some success to train multi-layer spiking networks. Alternative approaches using initial random dynamics coupled with error feedback and spike-based learning rules can permit recurrent SNNs to mimic a teacher dynamical system.^{30,31} Strictly-local spike-timing-based learning rules, inspired by results in experimental neuroscience,³² have been implemented in digital and mixed-signal neuromorphic devices, as they provide a better match to the distribution of information across neuromorphic chips.³³ Unfortunately, local spike-dependent rules such as Spike-Timing Dependent Plasticity (STDP) are themselves not able to provide supervised training of arbitrary tasks, since they do not permit error feedback or error-based modification of parameters. In both cases, implementing strictly local or backpropagation-based learning infrastructure on-chip adds considerable complexity, size and therefore cost to neuromorphic hardware designs. This cost makes it impractical to use on-chip learning and adaptation to solve the mismatch problem on mixed-signal architectures.

Robustness to noise and variability can be approached from the architectural side. For example, a network architecture search approach can identify networks that are essentially agnostic to precise weight values.³⁴ However, these networks rely on complex combinations of transfer functions which do not map to neuromorphic SNN designs. Alternatively, analytically-derived network architectures have been proposed for spiking networks,

relying on a balance between excitation and inhibition to provide robustness to sources of noise including spike-time stochasticity and neuron deletion.^{35–37} These networks, known as Efficient Balanced Networks (EBNs), can be derived to mimic an arbitrary linear dynamical system through an auto-encoding architecture³⁵ or can learn to represent and mimic dynamical systems.^{38–41} We propose to adapt the learning machinery of this spiking architecture to produce deployable SNN-based solutions for arbitrary supervised tasks that are robust to noise and device mismatch.

In this work we present a method for training robust networks of Leaky Integrate and Fire (LIF) spiking neurons that can solve supervised temporal signal regression and classification tasks. We adopt a knowledge distillation approach, by first training a non-spiking Recurrent Neural Network (RNN) to solve the desired supervised task using Back-Propagation Through Time (BPTT).²¹ By then interpreting the activations of the RNN as a teacher dynamical system, we train an SNN using an adaptation of the learning rule from ref. 39 to mimic the RNN. We show that the resulting trained SNN is robust to multiple forms of noise, including simulated device mismatch, making our approach feasible for deployment on to mixed-signal devices without post-deployment calibration or learning. We compare our method with several other standard approaches for configuring SNNs, and show that ours is more robust to device mismatch.

RESULTS

We assume a family of tasks defined by mappings $\mathbf{c}(t) \rightarrow \hat{\mathbf{y}}(t)$, where $\mathbf{c}(t) \in \mathbb{R}^{d1}$ and $\hat{\mathbf{y}}(t) \in \mathbb{R}^{d2}$ are temporal signals with arbitrary dimensionality (Figure 1a; see Methods). For simplicity of notation we do not write the temporal dependency “ (t) ” for the remainder of the paper. This definition encompasses any form of deterministic temporal signal processing or classification task without loss of generality. We refer to our network architecture as ADS (Arbitrary **D**ynamical **S**ystem) spiking networks.

Our approach begins by training a non-spiking rate network to implement

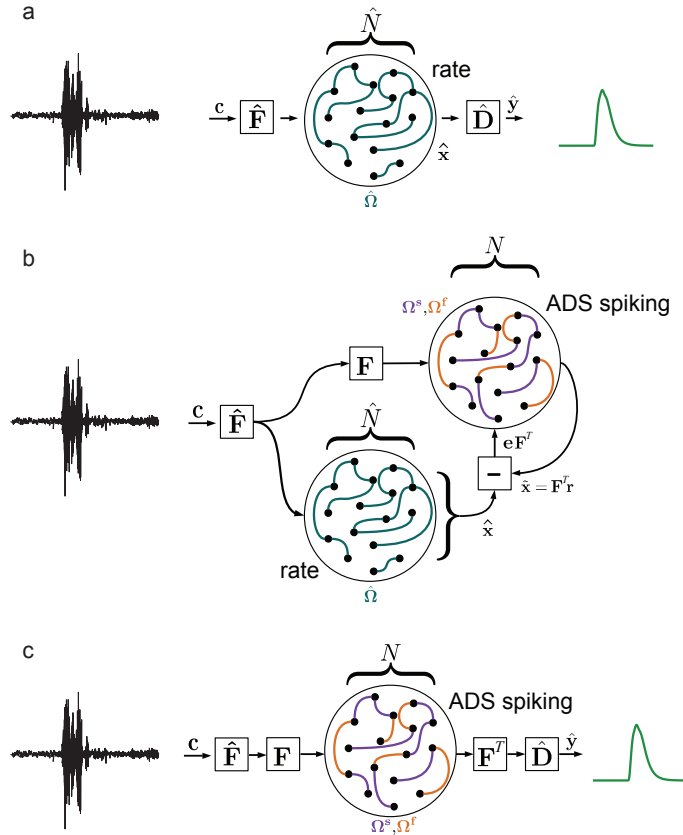


Fig. 1. Schematic overview of our supervised training approach. **a** A recurrent non-spiking neural network with \hat{N} neurons (“rate”) is trained using BPTT or a similar approach to implement the mapping $\mathbf{c} \rightarrow \hat{\mathbf{y}}$, via encoding and decoding weights $\hat{\mathbf{F}}$ and $\hat{\mathbf{D}}$, using the recurrent weights $\hat{\Omega}$ and resulting in the internal temporal representation of neural activity $\hat{\mathbf{x}}$. **b** To train a robust spiking network for the task, a network with $N \neq \hat{N}$ LIF neurons (“ADS spiking”) is initialised with fast balanced feedback connections Ω^f , analytically determined from a randomly chosen encoding matrix \mathbf{F} . The ADS spiking network learns to represent the target signals $\hat{\mathbf{x}}$ with reference to an error signal $\mathbf{e} = \hat{\mathbf{x}} - \hat{\mathbf{x}}$, by adapting slow feedback connections Ω^s . **c** For inference, the ADS spiking network replaces the non-spiking rate network, and uses the encoding and decoding weights $\hat{\mathbf{F}}$ and $\hat{\mathbf{D}}$ to implement the trained task mapping $\mathbf{c} \rightarrow \hat{\mathbf{y}}$.

the arbitrary task mapping by learning the dynamical system

$$\begin{aligned}\tau \dot{\hat{\mathbf{x}}} &= \hat{\Omega} f(\hat{\mathbf{x}}) + \hat{\mathbf{F}} \mathbf{c} + b \\ \hat{\mathbf{y}} &= \hat{\mathbf{D}} \hat{\mathbf{x}}\end{aligned}$$

through modification of the recurrent weights $\hat{\Omega} \in \mathbb{R}^{\hat{N} \times \hat{N}}$; encoding and decoding weights $\hat{\mathbf{F}} \in \mathbb{R}^{d1 \times \hat{N}}$ and $\hat{\mathbf{D}} \in \mathbb{R}^{\hat{N} \times d2}$; biases $b \in \mathbb{R}^{\hat{N}}$; time constants $\tau \in \mathbb{R}^{\hat{N}}$; and non-linear transfer function $f(\cdot) = \tanh(\cdot)$. BPTT or any other suitable approach can be used to obtain the trained rate network.

We subsequently train a network of spiking neurons to emulate $\hat{\mathbf{x}}$, with leaky membrane dynamics defined by

$$\dot{V} = -\lambda V + \hat{\mathbf{F}} \mathbf{F} \mathbf{c} - \Omega^f \mathbf{o} + \Omega^s \mathbf{o} + k \mathbf{F}^T \mathbf{e}$$

with spike trains $\mathbf{o} = V > V_{\text{thresh}}$ produced when exceeding threshold voltages V_{thresh} ; leak rate λ ; and fast and slow recurrent weights Ω^f and Ω^s (Figure 1b; see Methods). The decoded dynamics $\tilde{\mathbf{x}} \approx \hat{\mathbf{x}}$ are obtained from the filtered spiking activity \mathbf{r} with $\tilde{\mathbf{x}} = \mathbf{F} \mathbf{r}$. By feeding back an error signal $\mathbf{e} = \tilde{\mathbf{x}} - \hat{\mathbf{x}}$ under the control of a decaying feedback rate k , the spiking network is forced to remain close to the desired target dynamics. Ω^f is initialised to provide fast balanced feedback,³⁶ and Ω^s is learned using the rule

$$\dot{\Omega}^s = \eta \mathbf{r} \mathbf{F} \mathbf{e}$$

under learning rate η (see Methods and ref. 39). Note that we do not require complex multi-compartmental neurons or dendritic nonlinearities in our neuron model, but use a simple leaky integrate-and-fire neuron that is compatible with compact mixed-signal neuromorphic implementation.² Once the spiking network has learned to represent $\tilde{\mathbf{x}} \approx \hat{\mathbf{x}}$ with high accuracy, we replace the rate network entirely with the spiking network (Figure 1c).

Temporal XOR task

We begin by demonstrating our method using a nonlinear temporal XOR task (Figure 2; see Methods). This task requires memory of past inputs to produce a delayed output, as well as a nonlinear mapping between the memory state and the output variable. A network receives a single

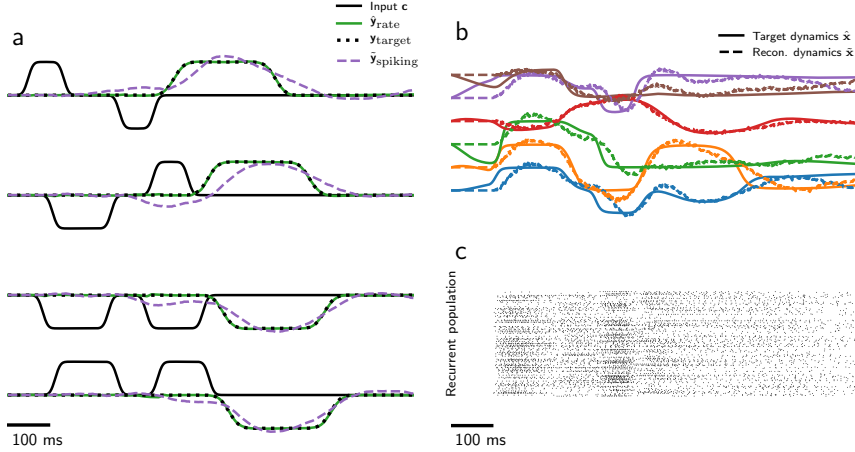


Fig. 2. **Our approach implements a supervised temporal non-linear sequence classification task to high accuracy.** **a** The non-spiking RNN (green; $\hat{N} = 64$ neurons) is trained to perform a temporal XOR of the input (black), closely matching the target function (dotted). A spiking ADS network (dashed; $N = 320$ neurons) is trained to perform the same task. **b** Selected internal dynamical variables \hat{x} of the RNN are shown (solid), along with their reconstructed equivalents \tilde{x} from the spiking ADS network (dashed). **c** The spiking activity of the ADS network. Panels **b** and **c** correspond to the first example in **a**.

input channel where pulses of varying width (100–230 ms) and sign are presented in sequence. The network must report the XOR of the two input pulses by delivering an output pulse of appropriate sign after the second of the two input pulses. A non-spiking RNN ($\hat{N} = 64$) was trained to perform the temporal XOR task, using BPTT with Mean-Squared Error (MSE) loss against the target output signal (target and output signals shown in Figure 2a). After 20 epochs of training with 500 samples per epoch, the RNN reached negligible error on 200 test samples ($\approx 100\%$ accuracy). A spiking ADS network ($N = 320$) was then trained to perform the task, reaching equivalent accuracy (Figure 2a, b).

Wake-phrase detection

The temporal XOR task demonstrates that one-dimensional nonlinear tasks requiring memory can be learned through our method through supervised training. To show that our approach also works on more realistic tasks with complex input dynamics, we implemented an audio wake-phrase

detection task (Figure 3; see Methods). Briefly, real-time audio signals were extracted from a database of spoken wake phrases (“Hey Snips” dataset⁴²), or from a database of noise samples (“DEMAND” dataset⁴³). The target wake phrase data was augmented with noise at an SNR of 10dB, then passed through a bank of 16 Butterworth filters with central frequencies spaced between 0.4 and 2.8 kHz (Figure 3b). We trained a non-spiking RNN ($\hat{N} = 128$) to perform the task with high accuracy, using BPTT under an MSE loss function against a smooth target classification signal (Figure 3d, e). We then trained a spiking ADS network ($N = 768$) to implement the audio classification task. While the non-spiking RNN achieved a testing accuracy of $\approx 90\%$, our spiking imitator achieved $\approx 87\%$ after training for 10 epochs on 1000 training samples.

Training considerations

We found that slower input, internal and target dynamics in the RNN were easier for the SNN to reconstruct than very rapid dynamics, depending on the neuron and synaptic time constants in the SNN. Longer and slower target responses yielded smoother ANN dynamics, which were easier for the spiking ADS network to learn. Our approach did not assume any dendritic non-linearities, or multi-compartmental dendrites with complex basis functions. Instead, the non-linearity of the spiking neuron dynamics is sufficient to learn the dynamics of a non-spiking ANN using the tanh nonlinearity.

We found that including a learning schedule for the error feedback rate k was important to achieve low reconstruction error. The factor k must drop to close to zero before the end of training, or else the SNN learns to rely on error feedback for accuracy, and generalisation will be poor once error feedback is removed. Conversely, if k drops too rapidly during training, the SNN is not held close to the desired target dynamics, and is unable to correctly learn the slow feedback weights Ω^s . For these reasons, a well-chosen schedule for k is important during learning. In this work we chose a progressive stepping function that decrements k by a fixed amount after some number of signal iterations (see Methods). Setting k to a fixed value for some number of trials enables the SNN to adapt to the corresponding scale of error feedback by updating Ω^s .

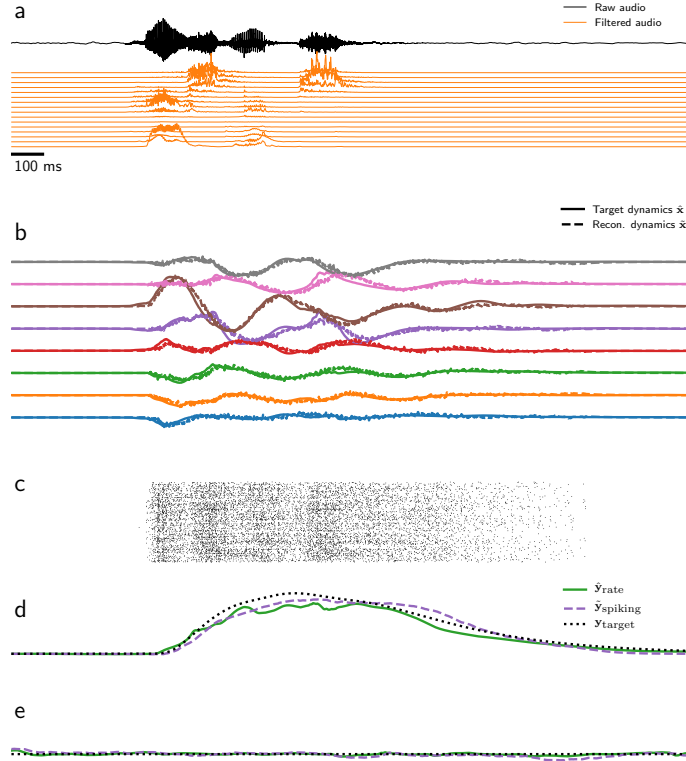


Fig. 3. Our approach performs a supervised spoken audio multi-dimensional classification task with high accuracy. **a** Audio samples were presented that either matched a spoken target phrase, or consisted of random speech or background noise. Raw audio (black) was filtered into 16 channels (orange) for classification by the network ($\mathbf{c} \in \mathbb{R}^{16}$). **b** Internal RNN dynamics ($\hat{\mathbf{x}}$; solid) was reconstructed accurately by the trained spiking ADS network ($\tilde{\mathbf{x}}$; dashed) based on the spiking activity (shown in **c**). An output signal was high (shown in **d**) when the audio sample matched the target signal, or low (shown in **e**) when the audio signal was background noise or other speech. Panels **a-d** correspond to a single trial.

Robustness to noise sources

The slow learned recurrent feedback connections Ω^s in the spiking network enables the SNN to reproduce a learned task. In contrast, the balanced fast recurrent feedback connections Ω^f are designed to enable the SNN to encode the dynamic variables $\tilde{\mathbf{x}}$ in a way that is robust to perturbation.^{35,36} We examined the robustness of our trained networks to several sources of noise (Figure 4).

Device Mismatch: We first introduced frozen parameter noise as a simulation of device mismatch present in mixed-signal neuromorphic implementation of event-driven neuron and synapses. We measured distributions of neuronal and synaptic parameters induced in silicon spiking neurons by device mismatch (see Methods; Figure S1). Measurements were performed on 1 core of 256 analog neurons and synapses, on fabricated mixed-signal neuromorphic DYNAP™-SE processors.² We observed a consistent relationship between the mean and variance of parameter distributions: the variance of the measured parameters increased linearly with the magnitude of the set parameter. We used this experimentally-recorded relationship to simulate mismatch in our spiking network implementations, simulating deployment of the networks on mixed-signal neuromorphic hardware. Mismatched parameters Θ' were generated with $\Theta' \sim \mathcal{N}(\Theta, \delta\Theta)$, where δ determines the level of mismatch, which we found experimentally to be between 10–20%. Under 20% simulated mismatch on weights, thresholds, biases, synaptic and neuronal time constants, our networks compensated well for the frozen parameter noise present in mixed-signal deployment (Figure 4b).

Quantisation Noise: In contrast to 64-bit floating point precision used by the non-spiking RNN, deployment of NN architectures in memory-constrained systems often uses low bit-depth precision for weights and neuron state. Mixed-signal neuromorphic architectures use analog voltages or currents to represent internal neural state, but can use some form of quantisation for synaptic weights. For example, DYNAP™-SE2 processors impose a five-bit representation of synaptic weights, as well as a restricted fan-in of 64 pre-synaptic input sources per neuron.² We imposed weight quantisation constraints on our spiking model, and found that our networks compensated well for the resulting frozen quantisation noise (Figure 4c; see Methods).

Thermal Noise: Due to the analog representation of neuron and synapse states in mixed-signal neuromorphic chips, these state variables are subject to thermal noise. Thermal noise appears as white-noise stochastic fluctuations of all states. We simulated thermal noise by adding noise $\zeta \sim \mathcal{N}(0, \sigma)$ to membrane potentials V , with $\sigma = 1\%, 5\%, 10\%$ scaled to the range between reset and threshold potentials V_{reset} and V_{thresh} . The

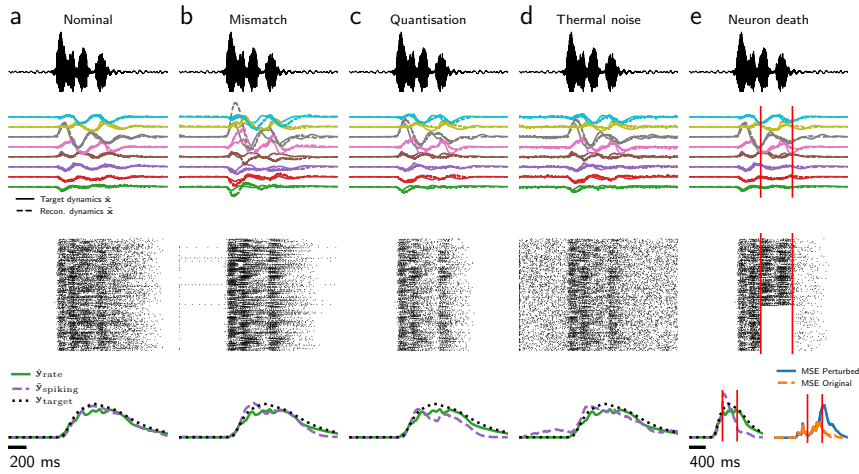


Fig. 4. Our trained spiking networks are robust to device mismatch and other sources of noise. Each column shows (top to bottom) the raw signal input; the ANN and reconstructed dynamics; the spiking activity of the ADS network; and the task output and target signals. **a** The trained ADS network reproduces the ANN internal and target signals with high accuracy. **b** In the presence of simulated mismatch in a mixed-signal silicon implementation of LIF neurons (20%; see Methods), the ADS network compensates well for the resulting frozen parameter noise. **c** Frozen weight noise introduced by quantisation of weights to 4 bits is compensated by the ADS spiking network. **d** The spiking network also compensates well in the presence of simulated thermal noise ($\sigma = 5\%$). **e** The balanced fast recurrent feedback connections Ω^f permit the ADS spiking network to compensate for sudden neuron death (40% of spiking neurons silenced between vertical bars).

spiking ADS network performed well in the presence of thermal noise (Figure 4d).

Sudden Neuron Failure: The fast recurrent feedback connections Ω^f present in spiking balanced networks have been shown to be able to compensate for neuron loss, where a subpopulation of spiking neurons is silenced during a trial.^{35,39,44} We examined this property in our spiking ADS networks that include fast balanced feedback, and found that indeed our networks compensated well for neuron loss (Figure 4e). In the absence of fast recurrent feedback (i.e. $\Omega^f = 0$), neuron silencing degraded the performance of the spiking ADS networks (Figure S3).

Comparison with alternative architectures

We have demonstrated that our method produces spiking implementations of arbitrary tasks, defined through supervised training. We compared our approach against several alternative methods for supervised training of SNNs, and evaluated the performance of these methods under simulated deployment on mixed-signal neuromorphic hardware:

- Reservoir Computing, in the form of a Liquid State Machine,¹⁸ relies on the random dynamics of an SNN to project an input over a high-dimensional temporal basis. A readout is then trained to map the random temporal basis to a specified target signal, using regularised linear regression. Since perturbation of the weights and neural parameters will directly modify the temporal basis, we expect the Reservoir approach to perform poorly in the presence of mismatch.
- The spiking FORCE algorithm³⁰ trains an SNN to mimic a teacher dynamical system. We applied this algorithm to a trained non-spiking RNNs to produce a trained SNN, similarly as in our spiking ADS approach.
- We implemented the BPTT algorithm to train an SNN end-to-end, using a surrogate gradient function similar to ref. 23. During training, these networks received input and target functions identical to those presented to the non-spiking RNN.

We first examined simulated deployment of all architectures by simulating parameter mismatch (Figure 5; see Methods). We trained 10 networks for each architecture, and evaluated each network at three levels of mismatch ($\delta = 5\%, 10\%, 20\%$) for 10 random mismatch trials of 500 samples each. We quantified the effect of mismatch on the performance of each network architecture by measuring the MSE between the SNN-generated output $\tilde{\mathbf{y}}$ and the training target for that architecture. For the FORCE and ADS networks the training target was the output of the non-spiking RNN \mathbf{y} . In the case of the Reservoir and BPTT architectures, the training target was the target task output $\hat{\mathbf{y}}$. Under the lowest level of simulated mismatch (5%), the spiking ADS network showed the smallest degradation of network response (MSE drop $0.0094 \rightarrow 0.0109$; $p \approx 8 \times 10^{-14}$, U test). The spiking ADS network also showed the smallest mismatched variance in MSE, reflecting that all mismatched networks responses were close to

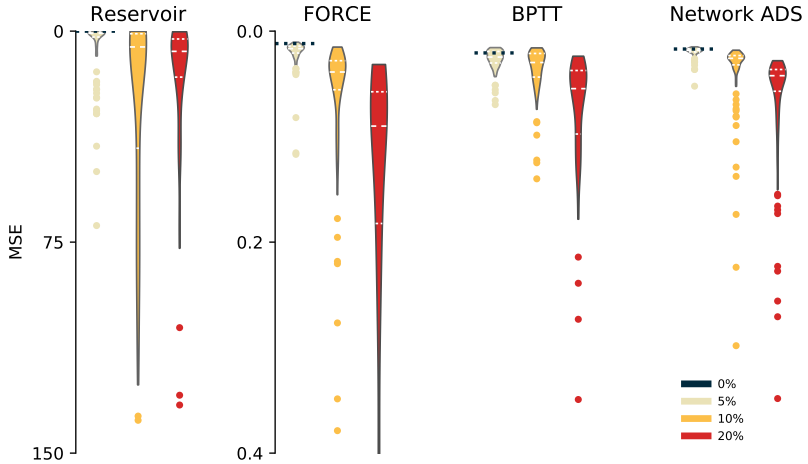


Fig. 5. Under simulated deployment, our method is more robust to mismatch than standard training approaches. Shown are the distributions of errors (MSE) between the non-spiking teacher RNN and final trained SNN response for 10 random initialisations of training for each architecture and 10 random instantiations for each level of mismatch. Dashed black line: baseline network with no mismatch ($\delta = 0\%$) for each architecture. See text for statistical comparisons.

the desired target response (MSE std. dev. ADS 0.0076; Reservoir 11.4; FORCE 0.0244; BPTT 0.0105; $p < 1 \times 10^{-2}$ in all cases, Levene test). The spiking Reservoir architecture fared the worst, with large degradation in MSE for even 5% mismatch (MSE drop $0.0157 \rightarrow 1.2523$; $p \approx 4 \times 10^{-51}$, U test). At 10% simulated mismatch, comparable with deployment on mixed-signal neuromorphic devices, our spiking ADS network architecture maintained the best MSE (ADS 0.0161; Reservoir 6.19; FORCE 0.301; BPTT 0.308), performing significantly better than all other architectures ($p < 1 \times 10^{-6}$ in all cases, U test). At 20% simulated mismatch the performance of all architectures began to degrade, but our spiking ADS architecture maintained the best MSE (ADS 0.0470; Reservoir 10.5; FORCE 0.953; BPTT 0.565; $p < 5 \times 10^{-2}$ in all cases, U test).

We compared the effect of quantisation noise on the four architectures, examining 6–2 bits of weight precision (Figure S2; see Methods). Note that no architectures were trained using quantisation-aware methods, making this a direct test of inherent robustness to quantisation noise. The Reservoir architecture broke down for any quantisation level (chance task performance accuracy $\approx 50\%$). The FORCE architecture performed

well down to 5 bits (median accuracy 85%), beyond which MSE increased and performance decayed to chance level at 3 bits (med. acc. 50%). Both the ADS spiking network and BPTT architectures maintained good performance down to 4 bits of precision (med. acc. ADS 81%; BPTT 87%), decaying to chance level at 2 bits (med. acc. ADS 52%; BPTT 54%).

We compared the effect of thermal noise of the four architectures, simulated as membrane potential noise (Figure S4; see Methods). The FORCE architecture was most robust to thermal noise, performing best at all noise levels (higher accuracy, $p < 5 \times 10^{-2}$; lower MSE, $p < 1 \times 10^{-3}$ except for highest level of noise; U tests). All other architectures degraded progressively with increasing noise levels. Our spiking ADS network architecture showed the smallest degradation in general over increasing noise levels (MSE 0.0083–0.115; acc. 82–67 %). The BPTT architecture also fared well, while dropping in accuracy for the largest noise level (med. acc. 56%).

DISCUSSION

We propose a method for supervised training of spiking neural networks that can be deployed on mixed-signal neuromorphic hardware without requiring per-device retraining or calibration. Our approach interprets the activity of a non-spiking RNN as a teacher dynamical system. Using results from dynamical systems learning theory, our spiking networks learn to copy the pre-trained RNN and therefore perform arbitrary tasks over temporal signals. Our method is able to produce spiking networks that perform both simple and complex non-linear temporal detection and classification tasks. We show that our networks are considerably more robust to several forms of parameter and state noise, compared with several other common techniques for training spiking networks.

Our networks are by design robust to common sources of network and parameter noise, which must be compensated for when deploying to mixed-signal neuromorphic hardware. For levels of mismatch measured directly from neuromorphic devices, we show that common SNN network architectures break down badly. Usual approaches for compensating for mismatch-induced parameter variation on neuromorphic hardware employ

either on-device training^{45–49} or per-device calibration,^{14, 15, 49–51} entailing considerable additional expense in hardware complexity or testing time. In contrast, our method produces spiking networks that do not require calibration or retraining to maintain performance after deployment. As a result, our approach provides a solution for cost-efficient deployment of event-driven neuromorphic hardware.

The coding scheme used by our spiking networks has been shown to promote sparse firing.³⁵ For mixed-signal neuromorphic hardware, power consumption is directly related to the network firing rate. Our method therefore produces networks that consume little power compared with alternative architectures that use firing-rate encoding or do not promote sparse activity.^{18, 21, 30}

Our approach to obtain high-performing SNNs is at heart a knowledge-transfer approach, relying on copying the dynamics of a highly-performing non-spiking RNN. This two-step approach is needed because the learning rule for our SNN requires a task to be defined in terms of a dynamical system, and is not able to learn the dynamics of an arbitrary input–output mapping (see Supplementary Methods). Consequently, our spiking networks can only perform as well as the pre-trained non-spiking RNN, and require multiple training steps to build a network for a new task. Nevertheless, training non-spiking RNNs is efficient when using automatic differentiation, just-in-time compilation and automatic batching,⁵² and can be performed rapidly on GPUs. Our approach trades off between training time on commodity hardware, and immediate deployment on neuromorphic hardware with no per-device training required.

The robustness of our spiking ADS networks comes partially from the fast balanced recurrent feedback connections, which ensure sparse encoding and compensate in real-time for encoding errors.^{35, 36} These weights also degrade under noise, but can be adapted in a local untrained fashion using local learning rules that are compatible with HW implementation.⁵³

Our supervised training approach is designed for temporal tasks, where input and target output signals evolve continuously. This set of tasks encompasses real-time ML-based signal processing and recognition, but is a poorer fit to high-resolution frame-based tasks such as frame-based

image processing. These “one-shot” tasks can be mapped into the temporal domain by serialising input frames⁵⁴ or by using temporal coding schemes.⁵⁵ We found anecdotally that temporal discontinuities in input and target time series made training our ADS networks more difficult, with the implication that a careful matching between task and network time constants is important.

Our approach builds single-population recurrent spiking networks, in contrast to deep non-recurrent network architectures which are common in 2021.⁵⁶ Recurrent spiking networks such as Liquid State Machines (LSMs) have been shown to be universal function approximators,⁵⁷ but RNNs do not perform the progressive task decomposition that can appear in deep feed-forward networks.⁵⁸ Interpretability of the internal state of recurrent networks such as ours is therefore potentially more difficult than for deep feedforward architectures.

Neuromorphic implementation of spiking neural networks has been hailed as the next generation of computing technology, with the potential to bring ultra-low-power non-von-Neumann computation to embedded devices. However, parameter mismatch has been a severe hurdle to large-scale deployment of mixed-signal neuromorphic hardware, as it directly attacks the reliability of the computational elements — a problem that commodity digital hardware generally does not face. Previous solutions to device mismatch have been impractical, as they require expensive per-device calibration or training prior to deployment, or increased hardware complexity (and therefore cost) in the form of on-device learning circuits. We have provided a programming method for mixed-signal neuromorphic hardware that frees application developers from the necessity to worry about computational unreliability, and does not require per-device handling during or after deployment. Our approach therefore removes a significant obstacle to the large-scale and low-cost deployment of neuromorphic devices.

METHODS

Temporal XOR task

We created signals of a total duration of 1 second, of which the first two thirds were dedicated to the input and the last third to the target (Figure 2). During the input time-frame, two activity bumps were created on a single input channel representing the binary inputs to the logical XOR operation. The bumps had varying length (uniformly drawn between 66–157 ms) and magnitude ± 1 , and were smoothed with a Gaussian filter to produce smooth activity transitions. In the final third of the signal we defined a target bump of magnitude ± 1 , indicating the true output of the XOR operation. The target bump was also smoothed with a Gaussian filter. We trained a rate network ($\hat{N} = 64$) to high performance on the XOR task, then subsequently trained a spiking model ($N = 320$) to follow the dynamics of the trained rate network. We used a fixed learning rate $\eta = 1 \times 10^{-5}$ and fixed error feedback rate $k = 75$ during SNN training. Output classification from both networks was determined by the network output passing the thresholds ± 0.5 .

Speech classification task

We drew samples from the “Hey Snips” dataset,⁴² augmented with noise samples from the DEMAND dataset,⁴³ with a signal-to-noise ratio of 10 dB. Each signal had a fixed length of 5 s and was pre-processed using a 16-channel bank of 2nd-order Butterworth filters with evenly-spaced centre frequencies ranging 0.4–2.8 kHz. The output of each filter was rectified with $\text{abs}(\cdot)$, then smoothed with a 2nd order Butterworth low-pass filter with cut-off frequency 0.3 kHz to provide an estimate of the instantaneous power in each frequency band. The rate network for the speech classification task ($\hat{N} = 128$) was trained for 1 epoch on 10 000 samples to achieve roughly the same performance as the spiking network trained with BPTT. We trained spiking networks ($N = 768$; $\tau_{\text{mem}} = 50$ ms; $\tau_{\text{fast}} = 1$ ms; $\tau_{\text{slow}} = 70$ ms) for 5 epochs on 1000 training samples, validated on 500 validation samples and 1000 test samples. To perform a classification we integrated the output of the network when it passed a threshold of 0.5.

We then applied a subsequent threshold on this integral, determined by a validation set, to determine the final prediction. We used a fixed learning rate $\eta = 1 \times 10^{-4}$ and a decaying step function for the error feedback factor k (from 200–25 in 8 evenly-spaced steps).

Spiking neuron model and initialisation

We used an LIF neuron model with a membrane time constant $\tau_{\text{mem}} = 50$ ms; reset potential $V_{\text{reset}} = 0$; resting potential $V_{\text{rest}} = 0.5$; and spiking threshold $V_{\text{thresh}} = 1$. The membrane potential dynamics for the neuron model were given by

$$\tau_{\text{mem}} \frac{\partial V}{\partial t} = V_{\text{rest}} - V + I_{\text{inp}} + I_{\text{fast}} + I_{\text{slow}} + I_{\mathbf{e}} + \eta_n$$

with input current I_{inp} ; fast and slow recurrent post-synaptic potentials (PSPs) I_{fast} and I_{slow} ; error current $I_{\mathbf{e}} = k \mathbf{D}^T \mathbf{e}$; and noise current η . Output spikes from a neuron are given by $o(t) = V > V_{\text{thresh}}$. Synaptic dynamics were described by

$$\tau_{\text{syn}} \frac{\partial I_*}{\partial t} = -I_* + (W \mathbf{o}(t) \tau_{\text{syn}}) / \Delta t$$

with input synaptic weights W ; synaptic time constants $\tau_{\text{syn}} = 1$ ms and 70 ms for fast and slow synapses, respectively; and simulation time step Δt . Feed-forward and decoding weights were initialised using a standard normal distribution scaled by the number of input/output dimensions (\hat{N}). Fast balanced recurrent feedback connections were initialised and rescaled according to the threshold and reset potential, as described in ref. 35. The spiking network was simulated using a forward Euler solver with a simulation time step of 1 ms.

Non-spiking network

The dynamics of a neuron in the non-spiking RNN were described by

$$\tau_j \dot{x}_j = -x_j + \hat{\mathbf{F}} c_j(t) + \hat{\Omega} f(\mathbf{x}) + b_j + \epsilon_j$$

with input $c(t)$; encoding weights $\hat{\mathbf{F}}$; recurrent weights $\hat{\Omega}$; non-linearity $f(\cdot) = \tanh(\cdot)$; bias b ; and noise term ϵ . Time constants τ were initialised with linearly spaced values (10–100 ms). The trainable parameters in this

network are the time constants τ ; the encoding and recurrent weights $\hat{\mathbf{F}}$ and $\hat{\Omega}$; and the biases b . No noise was applied during training or inference ($\epsilon = 0$).

Measurements of parameter mismatch

Using recordings from fabricated mixed-signal neuromorphic chips we measured levels of parameter mismatch (i.e. fixed substrate noise pattern) present in hardware. In particular, for DYNAPTM-SE,² a neuromorphic processor which emulates LIF neuron, AMPA and NMDA synapse models with analog circuits, we measured neuron and synaptic time constants, and synaptic weights for individual neuron units, by recording and analysing the voltage traces produced by these circuits. We observed levels of mismatch in the order of 10–20% for individual parameters, with widths of the distributions being proportional to the means (see Figure S1).

Simulated mismatch

To simulate parameter mismatch in mixed-signal neuromorphic hardware we derived a model where the values for each parameter follow a normal distribution with the standard deviation depending linearly on the mean. The mismatched parameters Θ' are obtained with $\Theta' \sim \mathcal{N}(\Theta, \delta\Theta)$ where δ determines the level of mismatch. We considered three levels of mismatch: 5, 10 and 20%.

Quantisation noise

We introduced quantisation noise by reducing the bit-precision of all weights post-training to 2,3,4,5 and 6 bits. The weights were quantised by setting $\mathbf{W}_{\text{disc}}^s = \rho \lfloor W/\rho \rfloor$ where $\rho = (\max(\mathbf{W}_{\text{full}}^s) - \min(\mathbf{W}_{\text{full}}^s))/(2^b - 1)$ and $\lfloor . \rfloor$ is the rounding operator.

Simulated thermal noise

Thermal noise is inherent in neuromorphic devices and can be modeled by Gaussian noise on the input currents. We applied three different levels

of thermal noise ($\sigma = 0.01, 0.05, 0.1$) that was scaled according to the difference between V_{reset} and V_{thresh} to assure equal amounts of noise for neuron model and network architecture.

Neuron silencing

We created four network instances grouped into two pairs: One pair was trained with the fast recurrent feedback connections Ω^f as described above, and the other pair with $\Omega^f = 0$. We then clamped 40% of the neurons of one instance of both pairs to V_{reset} while evaluating 1000 test samples.

Benchmark network architectures

We implemented a liquid state machine SNN;¹⁸ spiking FORCE network;³⁰ and a BPTT-trained SNN²¹ using Jax⁵² and custom-written forward-Euler solvers. Parameters for all architectures are given in the Supplementary Material, and code for all networks is available as part of Rockpool.⁵⁹

Statistical tests

All statistical comparisons were double-sided Mann-Whitney U tests unless stated otherwise.

ACKNOWLEDGEMENTS

This project has received funding in part by the European Union’s Horizon 2020 ERC project NeuroAgents (Grant No. 724295), from the European Union’s Horizon 2020 research and innovation programme for ECSEL grants ANDANTE (grant agreement No. 876925), TEMPO (grant agreement No. 826655), and SYNCH (grant agreement No. 824162).

AUTHOR CONTRIBUTIONS

The authors declare no competing interests.

DRM and GI conceived and designed the research. JB and DRM developed software and simulations. JB, SS and DZ performed experiments and collected data. JB and DRM analysed and interpreted the data. JB and DRM drafted the manuscript. DRM, JB, DZ, SS and GI performed critical revision of the manuscript. DRM approved the final version for publication.

ADDITIONAL INFORMATION

Supplementary Information is available for this paper.

Correspondence and requests for materials should be addressed to Dylan R Muir (dylan.muir@synsense.ai) and Julian Buchel (julian.buchel@synsense.ai).

Reprints and permissions information is available at www.nature.com/reprints.

DATA AVAILABILITY

Code to generate all models, analysis and figures in this paper are available from <https://github.com/jubueche/Robust-Classification-EBN>.

REFERENCES

- [1] Corradi, F. & Indiveri, G. A neuromorphic event-based neural recording system for smart brain-machine-interfaces. *IEEE Transactions on Biomedical Circuits and Systems* **9**, 699–709 (2015).
- [2] Moradi, S., Ning, Q., Stefanini, F. & Indiveri, G. A scalable multi-core architecture with heterogeneous memory structures for dynamic neuromorphic asynchronous processors (dynaps). *CoRR* **abs/1708.04198** (2017). 1708.04198.
- [3] Cassidy, A. S. *et al.* Truenorth: A high-performance, low-power neurosynaptic processor for multi-sensory perception, action, and cognition (2016).
- [4] Indiveri, G. *et al.* Neuromorphic silicon neuron circuits. *Frontiers in Neuroscience* **5**, 73 (2011). URL <https://www.frontiersin.org/article/10.3389/fnins.2011.00073>.
- [5] O’Connor, P., Neil, D., Liu, S.-C., Delbrück, T. & Pfeiffer, M. Real-time classification and sensor fusion with a spiking deep belief network. *Frontiers in Neuroscience* **7**, 178 (2013). URL <https://www.frontiersin.org/article/10.3389/fnins.2013.00178>.
- [6] Schemmel, J. *et al.* A wafer-scale neuromorphic hardware system for large-scale neural modeling. In *2010 IEEE International Symposium on Circuits and Systems (ISCAS)*, 1947–1950 (2010).

- [7] Davies, M. *et al.* Loihi: A neuromorphic manycore processor with on-chip learning. *IEEE Micro* **38**, 82–99 (2018).
- [8] Painkras, E. *et al.* Spinnaker: A 1-w 18-core system-on-chip for massively-parallel neural network simulation. *IEEE Journal of Solid-State Circuits* **48**, 1943–1953 (2013).
- [9] Mead, C. Neuromorphic electronic systems. In *Proc. IEEE*, 78:16291636 (1990).
- [10] Pelgrom, M., Duinmaijer, A. & Welbers, A. Matching properties of MOS transistors. *IEEE Journal of Solid-State Circuits* **24**, 1433–1440 (1989).
- [11] Tuinhout, H. & Wils, N. Parametric mismatch characterization for mixed-signal technologies. In *2009 IEEE Bipolar/BiCMOS Circuits and Technology Meeting*, 107–114 (2009).
- [12] Qiao, N. & Indiveri, G. Scaling mixed-signal neuromorphic processors to 28 nm fd-soi technologies. In *2016 IEEE Biomedical Circuits and Systems Conference (BioCAS)*, 552–555 (2016).
- [13] Indiveri, G. & Sandamirskaya, Y. The importance of space and time for signal processing in neuromorphic agents: The challenge of developing low-power, autonomous agents that interact with the environment. *IEEE Signal Processing Magazine* **36**, 16–28 (2019).
- [14] Neftci, E. & Indiveri, G. A device mismatch compensation method for vlsi neural networks. In *2010 Biomedical Circuits and Systems Conference (BioCAS)*, 262–265 (2010).
- [15] Aamir, S. A. *et al.* An accelerated lif neuronal network array for a large-scale mixed-signal neuromorphic architecture. *IEEE Transactions on Circuits and Systems I: Regular Papers* **65**, 4299–4312 (2018).
- [16] Sheik, S., Chicca, E. & Indiveri, G. Exploiting device mismatch in neuromorphic vlsi systems to implement axonal delays. In *IEEE International Joint Conference on Neural Networks (IJCNN) 2012*, Proceedings of the International Joint Conference on Neural Networks, 1–6 (IEEE, Brisbane, Australia, 2012). URL <https://doi.org/10.5167/uzh-75361>.
- [17] Yao, E., Hussain, S., Basu, A. & Huang, G.-B. Computation using mismatch: Neuromorphic extreme learning machines. 294–297 (2013).
- [18] Maass, W., Natschläger, T. & Markram, H. Real-time computing without stable states: A new framework for neural computation based on perturbations. *Neural Comput.* **14**, 2531–2560 (2002). URL <http://dx.doi.org/10.1162/089976602760407955>.
- [19] Eliasmith, C. A unified approach to building and controlling spiking attractor networks. *Neural Computation* **17**, 1276–1314 (2005). URL <https://doi.org/10.1162/0899766053630332>. <https://doi.org/10.1162/0899766053630332>.
- [20] Krizhevsky, A., Sutskever, I. & Hinton, G. E. Imagenet classification with deep convolutional neural networks. *Commun. ACM* **60**, 84–90 (2017). URL <https://doi.org/10.1145/3065386>.
- [21] Werbos, P. J. Backpropagation through time: what it does and how to do it. *Proceedings of the IEEE* **78**, 1550–1560 (1990).
- [22] Lee, J. H., Delbrück, T. & Pfeiffer, M. Training deep spiking neural networks using backpropagation. *Frontiers in Neuroscience* **10**, 508 (2016). URL <https://www.frontiersin.org/article/10.3389/fnins.2016.00508>.
- [23] Neftci, E. O., Augustine, C., Paul, S. & Detorakis, G. Event-driven random

back-propagation: Enabling neuromorphic deep learning machines. *Frontiers in Neuroscience* **11**, 324 (2017). URL <https://www.frontiersin.org/article/10.3389/fnins.2017.00324>.

[24] Bellec, G. *et al.* A solution to the learning dilemma for recurrent networks of spiking neurons. *Nature Communications* **11**, 3625 (2020). URL <https://doi.org/10.1038/s41467-020-17236-y>.

[25] Neftci, E. O., Mostafa, H. & Zenke, F. Surrogate gradient learning in spiking neural networks. *CoRR* **abs/1901.09948** (2019). URL <http://arxiv.org/abs/1901.09948>.

[26] Gerstner, W., Lehmann, M., Liakoni, V., Corneil, D. & Brea, J. Eligibility traces and plasticity on behavioral time scales: Experimental support of neohebbian three-factor learning rules. *Frontiers in Neural Circuits* **12**, 53 (2018). URL <https://www.frontiersin.org/article/10.3389/fncir.2018.00053>.

[27] Wunderlich, T. C. & Pehle, C. Eventprop: Backpropagation for exact gradients in spiking neural networks (2020). [2009.08378](https://arxiv.org/abs/2009.08378).

[28] Lillicrap, T. P., Cownden, D., Tweed, D. B. & Akerman, C. J. Random synaptic feedback weights support error backpropagation for deep learning. *Nature Communications* **7**, 13276 (2016). URL <https://doi.org/10.1038/ncomms13276>.

[29] Kaiser, J., Mostafa, H. & Neftci, E. Synaptic plasticity dynamics for deep continuous local learning (decolle). *Frontiers in Neuroscience* **14** (2020). URL <http://dx.doi.org/10.3389/fnins.2020.00424>.

[30] Nicola, W. & Clopath, C. Supervised learning in spiking neural networks with force training. *Nature Communications* **8**, 2208 (2017). URL <https://doi.org/10.1038/s41467-017-01827-3>.

[31] Gilra, A. & Gerstner, W. Predicting non-linear dynamics by stable local learning in a recurrent spiking neural network. *eLife* **6** (2017).

[32] Markram, H., Gerstner, W. & Sjöström, P. J. Spike-timing-dependent plasticity: a comprehensive overview. *Frontiers in synaptic neuroscience* **4**, 2–2 (2012). URL <https://pubmed.ncbi.nlm.nih.gov/22807913/>. 22807913[pmid].

[33] Brader, J. M., Senn, W. & Fusi, S. Learning real-world stimuli in a neural network with spike-driven synaptic dynamics. *Neural Comput* **19**, 2881–2912 (2007).

[34] Gaier, A. & Ha, D. Weight agnostic neural networks. In *Advances in Neural Information Processing Systems*, 5364–5378 (2019).

[35] Boerlin, M., Machens, C. K. & Denève, S. Predictive coding of dynamical variables in balanced spiking networks. *PLOS Computational Biology* **9**, 1–16 (2013). URL <https://doi.org/10.1371/journal.pcbi.1003258>.

[36] Denève, S. & Machens, C. K. Efficient codes and balanced networks. *Nature Neuroscience* **19**, 375–382 (2016). URL <https://doi.org/10.1038/nn.4243>.

[37] Calaim, N., Alexander Dehmelt, F., Gonçalves, P. J. & Machens, C. K. Robust coding with spiking networks: a geometric perspective. *bioRxiv* (2020).

[38] Bourdoukan, R., Barrett, D. G. T., Machens, C. K. & Denève, S. Learning optimal spike-based representations. In *Proceedings of the 25th International Conference on Neural Information Processing Systems - Volume 2*, NIPS'12, 2285–2293 (Curran Associates Inc., USA, 2012). URL <http://dl.acm.org/citation.cfm?id=2999325.2999390>.

[39] Alemi, A., Machens, C. K., Denève, S. & Slotine, J.-J. E. Learning nonlinear dynamics

in efficient, balanced spiking networks using local plasticity rules. In *AAAI*, 588–595 (2018). URL <https://www.aaai.org/ocs/index.php/AAAI/AAAI18/paper/view/17438>.

[40] Denève, S., Alemi, A. & Bourdoukan, R. The brain as an efficient and robust adaptive learner. *Neuron* **94**, 969 – 977 (2017). URL <http://www.sciencedirect.com/science/article/pii/S0896627317304178>.

[41] Brendel, W., Bourdoukan, R., Vertechi, P., Machens, C. K. & Denève, S. Learning to represent signals spike by spike. *PLoS Comput. Biol.* **16**, e1007692 (2020).

[42] Coucke, A. *et al.* Efficient keyword spotting using dilated convolutions and gating. *CoRR* **abs/1811.07684** (2018). URL <http://arxiv.org/abs/1811.07684>. 1811.07684.

[43] Thiemann, J., Ito, N. & Vincent, E. DEMAND: a collection of multi-channel recordings of acoustic noise in diverse environments (2013). URL <https://doi.org/10.5281/zenodo.1227121>. Supported by Inria under the Associate Team Program VERSAMUS.

[44] Barrett, D. G., Denève, S. & Machens, C. K. Optimal compensation for neuron loss. *eLife* **5**, e12454 (2016). URL <https://doi.org/10.7554/eLife.12454>.

[45] Fusi, S., Annunziato, M., Badoni, D., Salamon, A. & Amit, D. J. Spike-driven synaptic plasticity: Theory, simulation, vlsi implementation. *Neural Computation* **12**, 2227–2258 (2000). URL <https://doi.org/10.1162/089976600300014917>. <https://doi.org/10.1162/089976600300014917>.

[46] Cameron, K. & Murray, A. Minimizing the effect of process mismatch in a neuromorphic system using spike-timing-dependent adaptation. *IEEE Transactions on Neural Networks* **19**, 899–913 (2008).

[47] Mitra, S., Fusi, S. & Indiveri, G. Real-time classification of complex patterns using spike-based learning in neuromorphic vlsi. *IEEE Transactions on Biomedical Circuits and Systems* **3**, 32–42 (2009).

[48] Pfeil, T., Scherzer, A., Schemmel, J. & Meier, K. Neuromorphic learning towards nano second precision. In *The 2013 International Joint Conference on Neural Networks (IJCNN)*, 1–5 (2013).

[49] Wunderlich, T. *et al.* Demonstrating advantages of neuromorphic computation: A pilot study. *Frontiers in Neuroscience* **13**, 260 (2019). URL <https://www.frontiersin.org/article/10.3389/fnins.2019.00260>.

[50] Costas-Santos, J., Serrano-Gotarredona, T., Serrano-Gotarredona, R. & Linares-Barranco, B. A spatial contrast retina with on-chip calibration for neuromorphic spike-based aer vision systems. *IEEE Transactions on Circuits and Systems I: Regular Papers* **54**, 1444–1458 (2007).

[51] Neftci, E., Chicca, E., Indiveri, G. & Douglas, R. A systematic method for configuring vlsi networks of spiking neurons. *Neural Computation* **23**, 2457–2497 (2011). URL https://doi.org/10.1162/NECO_a_00182. PMID: 21732859, https://doi.org/10.1162/NECO_a_00182.

[52] Bradbury, J. *et al.* JAX: composable transformations of Python+NumPy programs (2018). URL <http://github.com/google/jax>.

[53] Büchel, J., Kakon, J., Perez, M. & Indiveri, G. Implementing efficient balanced networks with mixed-signal spike-based learning circuits (2020). 2010.14353.

[54] Le, Q. V., Jaitly, N. & Hinton, G. E. A simple way to initialize recurrent networks of rectified linear units (2015). 1504.00941.

[55] Thorpe, S., Delorme, A. & Van Rullen, R. Spike-based strategies for rapid processing.

Neural Networks **14**, 715 – 725 (2001). URL <http://www.sciencedirect.com/science/article/pii/S0893608001000831>.

- [56] Sengupta, S. *et al.* A review of deep learning with special emphasis on architectures, applications and recent trends. *Knowledge-Based Systems* **194**, 105596 (2020). URL <http://www.sciencedirect.com/science/article/pii/S095070512030071X>.
- [57] Maass, W. & Markram, H. On the computational power of circuits of spiking neurons. *Journal of Computer and System Sciences* **69**, 593 – 616 (2004). URL <http://www.sciencedirect.com/science/article/pii/S0022000004000406>.
- [58] Montavon, G., Samek, W. & Müller, K.-R. Methods for interpreting and understanding deep neural networks. *Digital Signal Processing* **73**, 1 – 15 (2018). URL <http://www.sciencedirect.com/science/article/pii/S1051200417302385>.
- [59] Muir, D., Bauer, F. & Weidel, P. Rockpool documentataton (2019). URL <https://doi.org/10.5281/zenodo.4045345>.

SUPPLEMENTARY MATERIAL

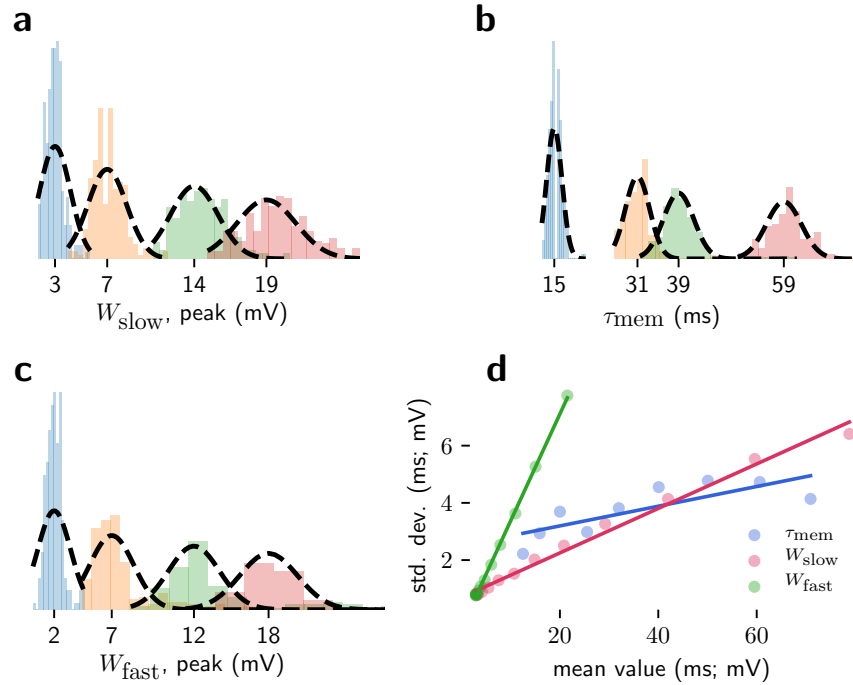


Fig. S1. Neuronal and synaptic parameter mismatch on mixed-signal Neuromorphic devices follow a mean-to-variance linear scaling rule. Measurements of actual weights of two types of silicon synapses with slow (a) and fast dynamics (c), as well as neuron time constants (b), show a consistent linear relationship between nominal set value and the distribution of actual mismatch parameter values. In all cases, the variance of measured parameters scaled with the nominal set value (d) (linear regression $r = 0.79$ τ_{mem} ; $r = 0.994$ W_{slow} ; $r = 0.9996$ W_{fast}).

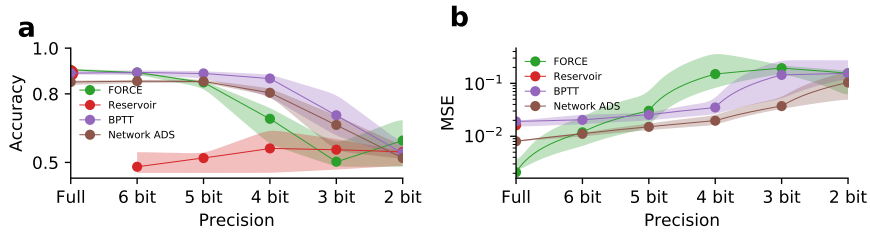


Fig. S2. Our method is more robust to quantisation noise than other standard training approaches. Median and IQR for accuracy (a) and MSE (b) for four network architectures. The weights of 10 networks for each architecture were quantised to the bit-depths indicated, then evaluated on 1000 test samples each. Reservoir performance degraded completely for all quantisation bit-depths (very high MSE) so is not indicated in b.

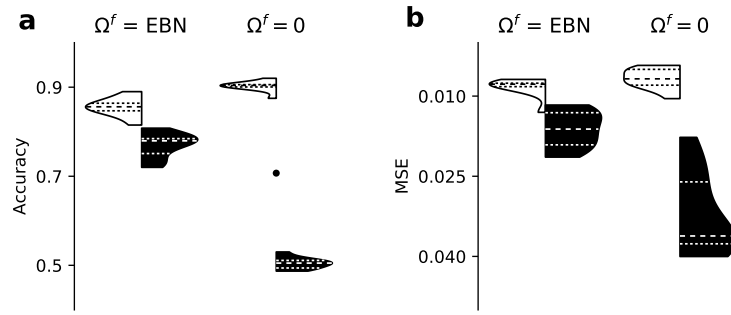


Fig. S3. Fast balanced feedback Ω^f provides robustness to neuron silencing. The effect of silencing 40% of neurons in spiking ADS networks is shown on accuracy (a) and on output error MSE (b). White: Network performance without silencing. Black: Network performance when silencing 40% of spiking neurons. Fast balanced recurrent feedback ($\Omega^f = \text{EBN}$) provided robustness to neuron silencing (small drop in performance). Networks without fast balanced recurrent feedback ($\Omega^f = 0$) exhibited more severe performance degradation under neuron silencing (large drop in performance).

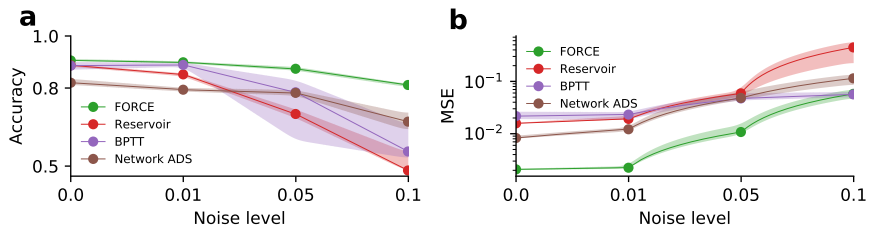


Fig. S4. **Effect of membrane potential noise on network responses.** Median and IQR for accuracy (a) and MSE (b) for four network architectures. Noise was added to 10 instances of each network architecture, as Normally-distributed noise with std. dev. σ scaled to the range between V_{thresh} and V_{reset} for each neuron (see Methods).

SUPPLEMENTARY METHODS

Learning in adaptive non-linear control theory

Let us assume an arbitrary dynamical system of the form

$$\dot{\mathbf{x}}(t) = f(\mathbf{x}(t)) + \mathbf{c}(t) \quad (1)$$

where $\mathbf{x}(t)$ is a vector of state variables $x_j(t)$, $f(\cdot)$ is a non-linear function (e.g. $\tanh(\cdot)$), and $\mathbf{c}(t)$ is a time-dependent input of the same dimensionality of $\mathbf{x}(t)$. Furthermore, let us assume a "student" dynamical system of the form

$$\dot{\hat{\mathbf{x}}}(t) = -\lambda \hat{\mathbf{x}}(t) + \mathbf{W}^T \Psi(\hat{\mathbf{x}}(t)) + \mathbf{c}(t) + k \cdot \mathbf{e}(t) \quad (2)$$

where $\hat{\mathbf{x}}(t)$ is a vector of state variables $\hat{x}_j(t)$, λ is a leak term, and $\mathbf{c}(t)$ is the same time-dependent input as in Equation 1. Over time, the signed error $\mathbf{e}(t) = \mathbf{x}(t) - \hat{\mathbf{x}}(t)$ between the teacher dynamics (Eq. 1) and the student dynamics (Eq. 2) is computed and fed into the student dynamics, causing the student state variables $\hat{\mathbf{x}}(t)$ to closely follow the target variables $\mathbf{x}(t)$.

This close tracking enables us to update the weights \mathbf{W} using Eq. 3, so that over the course of learning, the factor k can be reduced to zero and the network follows the teacher dynamics autonomously, using only a weighted sum of basis functions, given by $\Psi(\hat{\mathbf{x}}(t)) = \phi(\mathbf{M}\hat{\mathbf{x}}(t) + \theta)$, for some non-linear function ϕ , and some random \mathbf{M} and θ .

The learning rule used to adapt the weights \mathbf{W} is given by

$$\dot{\mathbf{W}} = \eta \Psi(\hat{\mathbf{x}}(t)) \mathbf{e}(t)^T \quad (3)$$

and can be shown to let the weights \mathbf{W} converge towards the optimal weights, denoted \mathbf{W}^{true} , assuming that the input $\mathbf{c}(t)$ does not lie on a low-dimensional manifold and that the student system has enough high-dimensional basis functions. For more information and a proof of the above statement, see ref. 39

It should be noted that the relation between $x(t)$ and $c(t)$ should be well-defined by an autonomous (non-)linear dynamical system of the form $\dot{\mathbf{x}}(t) = f(\mathbf{x}(t)) + \mathbf{c}(t)$ and that one cannot simply assume a "black box" dynamical system implementing *any* relation of the form $\dot{\mathbf{x}}(t) = \mathcal{B}(\mathbf{x}(t), \mathbf{x}(t))$. Concretely, in the light of classification, one cannot simply

assume there exists an autonomous dynamical system relating the input $\mathbf{c}(t)$ to some target response variable, and that this relation can be learned by the learning rule described above. This observation is important, as it makes it harder to build a classifier given the tools described above. In the next section, we will review how a network of spiking neurons can implement the above learning rule in order to learn the dynamics of a teacher dynamical system.

Learning arbitrary dynamical systems in Efficient Balanced Networks (EBNs)

In this section, we will briefly recapitulate how an EBN of spiking neurons can learn to implement any non-linear dynamical system of the form $\dot{\mathbf{x}}(t) = f(\mathbf{x}) + \mathbf{c}(t)$. We will assume that, given a network of N neurons, one can use a decoder \mathbf{D} to reconstruct the target variable from the filtered spike trains of the population using $\hat{\mathbf{x}}(t) = \mathbf{D}\mathbf{r}(t)$, so that $\mathbf{x}(t) \approx \hat{\mathbf{x}}(t)$.

Derived from the fact that in an EBN a neuron only fires a spike if it contributes to reducing the loss L ,^{35,38} given by

$$L = \frac{1}{T} \sum_{t=0}^T \|\mathbf{x}(t) - \hat{\mathbf{x}}(t)\|_2^2 + \mu\|\mathbf{r}(t)\|_2^2 + \nu\|\mathbf{r}(t)\|_1$$

with smoothed firing rates $\mathbf{r}(t)$ and loss regularisation terms μ and ν , the membrane potentials in the network are then given by

$$V(t) = \mathbf{D}^T \mathbf{x}(t) - \mathbf{D}^T \mathbf{D}\mathbf{r}(t) - \mu\mathbf{r}(t) \quad (4)$$

Following ref. 39, we differentiate Eq. 4 and substitute the smoothed firing rates $\dot{\mathbf{r}}(t) = -\lambda\mathbf{r}(t) + \mathbf{o}(t)$; the teacher dynamics $\dot{\mathbf{x}}(t) = f(\mathbf{x}(t)) + \mathbf{c}(t)$; and the decoded dynamics of the student $\dot{\hat{\mathbf{x}}}(t) = \mathbf{D}\dot{\mathbf{r}}(t)$, to obtain

$$\begin{aligned} \dot{V}(t) &= -\lambda V(t) + \mathbf{D}^T (f(\mathbf{x}(t) + \mathbf{c}(t))) - \mathbf{D}^T \mathbf{D}(-\lambda\mathbf{r}(t) + \mathbf{o}(t)) - \mu(-\lambda\mathbf{r}(t) + \mathbf{o}(t)) \\ &= -\lambda V(t) + \mathbf{D}^T \mathbf{c}(t) - (\mathbf{D}^T \mathbf{D} + \mu\mathbf{I})\mathbf{o}(t) + \mathbf{D}^T (\lambda\mathbf{x}(t) + f(\mathbf{x}(t))) \end{aligned}$$

with decay rates λ ; population spike trains $\mathbf{o} = V > V_{\text{thresh}}$; and identity matrix \mathbf{I} .

Under the non-linear control learning theoretical result of ref. 39, the term $\lambda\mathbf{x}(t) + f(\mathbf{x}(t))$ is approximated by a weighted set of basis functions over

slow recurrent feedback weights Ω^s , given by $\Omega^s \Psi(\mathbf{r}(t))$, where $\Psi(\mathbf{r}(t)) = \phi(\mathbf{M}\mathbf{r}(t) + \theta)$, inspired by complex multi-compartmental dendritic dynamics. In our networks we omitted the term $\Psi(\mathbf{r}(t))$ and simply replaced it with the population spike train $\mathbf{o}(t)$.

By feeding the error term $\mathbf{e}(t) = \mathbf{x}(t) - \hat{\mathbf{x}}(t)$ back into the network using the encoding/decoding weights \mathbf{D}^T , we obtain the final network dynamics

$$\dot{V}(t) = -\lambda V(t) + \mathbf{F}\mathbf{c}(t) - \Omega^f \mathbf{o}(t) + \Omega^s \mathbf{o}(t) + k \mathbf{D}^T \mathbf{e}(t)$$

where the encoding weights \mathbf{F} are given by \mathbf{D}^T and the optimal fast recurrent weights by $\Omega^f = -(\mathbf{D}^T \mathbf{D} + \mu \mathbf{I})$.³⁵

Similar to the case in control-theory, the learning rule for the slow recurrent weights is given by

$$\dot{\Omega}^s = \eta \Psi(\mathbf{r}(t)) (\mathbf{D}^T \mathbf{e}(t))^T$$

where we simply replaced $\Psi(\mathbf{r}(t))$ with $\mathbf{r}(t)$.

To speed up the simulations, one could assume that the accumulated updates to Ω^s , given by $\sum_{t=0}^T \eta \mathbf{r}(t) (\mathbf{D}^T \mathbf{e}(t))^T$ are approximately the same as accumulating the rates and errors into large arrays of size $N \times T$ and performing the update in a batched fashion, after a whole signal was evaluated rather than after every time-step, using

$$\dot{\Omega}^s = \eta \mathbf{r} (\mathbf{D}^T \mathbf{e})^T$$

We verified experimentally that this method is indeed faster, but yields less optimal results.

Spiking ADS network connectivity

The decoder weights, denoted \mathbf{D} , are initialised using a standard normal distribution $\mathcal{N}(0, 1/N_c)$, where N_c is the dimensionality of the input signal. The encoding weights \mathbf{F} are given by simply transposing the decoding weights such that $\mathbf{F} = \mathbf{D}^T$.

Unless stated otherwise, the slow recurrent connections were initialized using a zero matrix: $\Omega^s = \mathbf{0}$.

Following the optimal network connectivity of EBNs,³⁵ we initialized $\Omega^{\mathbf{f}_*}$ with $\mathbf{D}^T \mathbf{D} + \mu \lambda_d^2 \mathbf{I}$, which was then transformed to $\Omega^{\mathbf{f}}$ using

$$\Omega^{\mathbf{f}} = \frac{\xi a}{\tau_{\text{fast}}} \Omega^{\mathbf{f}_*} / V_{\text{thresh}}^*$$

where

$$V_{\text{thresh},n}^* = \frac{\nu \lambda_d + \mu \lambda_d^2 + \|D_n\|_2^2}{2}$$

with $\mu = 0.0005$, $\nu = 0.0001$, $\lambda_d = 20$, $\xi = 10$, and $a = 0.5$.

We applied the transformation described in the section “Scaling and physical units” in ref.³⁵ to transform our network to have $V_{\text{reset}} = 0$ and $V_{\text{thresh}} = 1.0$.

Training an EBN-based classifier

The coding properties of EBNs make them attractive for many applications, especially in the neuromorphic community. However, so far it has only been shown how to implement linear and non-linear dynamical systems of a specific form using EBNs. In this section we provide a method to train an EBN to perform classification tasks of varying complexity.

Let us define our time-varying, real-valued input as $\mathbf{c}(t)$, where $\mathbf{c} \in \mathcal{R}^{N_c \times 1}$ and $t \in \{0 \dots T\}$. The goal of training a classifier is to find a mapping $f(\mathbf{c}, \Theta) \rightarrow \mathbf{y}$ that maps any input \mathbf{c} to the desired target variable \mathbf{y} , where \mathbf{y} is a variable over time indicating the target and Θ is the set of system parameters. For simplicity, we will consider the case of binary classification. We however note that our method can be easily extended to a multi-class classification task.

Considering the ability of the learning rule presented in section , one might be inclined to assume a “black box” dynamical system \mathcal{B} of the form $\dot{\mathbf{y}}(t) = f(\mathbf{y}(t)) + \mathbf{c}(t)$ that, given input \mathbf{c} , autonomously produces the desired target \mathbf{y} . Two problems come with this approach:

- 1) The dynamical system is not well-defined, as it is no-longer explicitly defined by a teacher dynamical system. Furthermore, the system is autonomous, as the function $f(\cdot)$ does not depend on the input, but

only on past values of the target variable, making it impossible for the system to find a complex relationship between input and target.

2) This approach assumes that the input and target variable have the same number of dimensions, which is almost never the case.

How can we use the above learning rule to train an EBN to perform arbitrary classification tasks at low metabolic cost, high robustness and good classification performance? To answer this question, we consider a simple RNN comprising \hat{N} units, following

$$\tau_j \dot{x}_j(t) = -x_j(t) + \hat{\mathbf{F}}c(t)_j + \hat{\Omega}f(x(t))_j + b_j + \epsilon_j \quad (5)$$

where τ_j is the time constant of the j -th unit; $\hat{\mathbf{F}}$ are feed-forward encoding weights of shape $\hat{N} \times N_c$; $c(t)$ is the N_c dimensional input at time t ; $f(\cdot)$ is a non-linear function (e.g. $\tanh(\cdot)$); $\hat{\Omega}$ are recurrent weights of shape $\hat{N} \times \hat{N}$; and b_j and ϵ_j are bias and noise terms, respectively.

We observe that an RNN can be rewritten in the general form

$$\begin{aligned} \dot{\mathbf{x}}(t) &= \tilde{f}(\mathbf{x}) + \tilde{\mathbf{c}}(t), \text{ with} \\ \tilde{f}(\mathbf{x}) &= 1/\tau(-\mathbf{x}(t) + \hat{\Omega}f(\mathbf{x}(t)) + \epsilon) \text{ and} \\ \tilde{\mathbf{c}}(t) &= 1/\tau(\hat{\mathbf{F}}\mathbf{c}(t) + \mathbf{b}), \end{aligned}$$

implying that an EBN can be trained to implement the dynamics of *any* given RNN obeying the dynamics of Eq. 5.

Let us now restate the dynamics of the spiking network with adapted notation for ease of understanding:

$$\dot{V}(t) = -\lambda V(t) + \mathbf{F}\tilde{\mathbf{c}}(t) - \Omega^f \mathbf{o}(t) + \Omega^s \mathbf{o}(t) + k \mathbf{D}^T \mathbf{e}(t)$$

And let us assume that we have trained an RNN receiving inputs \mathbf{c} to successfully produce a good approximation $\hat{\mathbf{y}} = \hat{\mathbf{D}}\mathbf{x}$ of the target \mathbf{y} , so that $\hat{\mathbf{y}} \approx \mathbf{y}$.

We now see that we can train a network of spiking neurons to encode the *dynamics* \mathbf{x} of the RNN, by giving the spiking network input $\tilde{\mathbf{c}}(t) = 1/\tau(\hat{\mathbf{F}}\mathbf{c}(t) + \mathbf{b})$. This makes the *dynamics* of the RNN the new target of the spiking network: $\tilde{\mathbf{x}} = \mathbf{D}\mathbf{r}$, so that $\tilde{\mathbf{x}} \approx \mathbf{x}$. After the recurrent weights Ω^s have been learned to implement a network that encodes the rate-network dynamics, classification can be performed by the simple computation

$y(t) = \hat{\mathbf{D}}\mathbf{Dr}(t)$, where $\hat{\mathbf{D}}$ are the rate-network read-out weights, \mathbf{D} are the spiking read-out weights and $\mathbf{r}(t)$ are the filtered spike trains at time t of the spiking network.

Simulation and Learning

To simulate our network, we used a Jax⁵² implementation. In all experiments, we used a simple Euler integration method with a time-step of 1 ms.

To ensure that during learning the reconstructed dynamics closely follow the target dynamics, the term $\mathbf{e} = \mathbf{x} - \hat{\mathbf{x}}$ is computed and fed back into the network using the feedforward weights $I_{k\mathbf{D}^T\mathbf{e}} = k\mathbf{Fe}$. The error was then used to compute the update of the slow recurrent weights according to $\dot{\Omega}^s = \eta \mathbf{r}(t)(\mathbf{D}^T \mathbf{e}(t))^T$. In the batched-update version, the filtered spike trains $\mathbf{r}(t)$ and errors $\mathbf{e}(t)$ are then collected in two matrices – $\mathbf{R} \in \mathcal{R}^{N \times T}$ and $\mathbf{E} \in \mathcal{R}^{\hat{N} \times T}$ – which are then used to compute the update $\dot{\Omega}^s = \mathbf{R}(\mathbf{FE})^T$. In light of the constraint of some neuromorphic chips that reset potentials can not be calibrated on a per-neuron basis, we did not permit updates to the diagonal of Ω^s , which was always set to zero. To furthermore avoid uneven update magnitudes due to the richness of the input (some input signals have only short periods of sound, while others – typically the negative samples – have long ones) we normalised $\dot{\Omega}^s$ by $(\sum_i \sum_j \dot{\Omega}_{i,j}^s)/N^2$. Note that this only applies to the batched update case, which we did not use in the experiments.

Finally, the slow recurrent weights are updated according to

$$\Omega^s = \Omega^s + \eta \dot{\Omega}^s$$

where $\eta = 1 \times 10^{-5}$ for the audio task and $\eta = 5 \times 10^{-6}$ for the temporal XOR task.

Temporal XOR task

In this experiment, we trained an RNN with $\hat{N} = 64$ units to implement a classifier for the temporal XOR task. This task consists of a one-dimensional temporal signal comprising two sequentially-presented inputs

of varying sign to be classified according to the logical operator XOR. The result of the XOR is signalled by an output (and target) signal which is zero until the withdrawal of the second input, after which the output should go to ± 1 to indicate the result of the XOR. For example, a signal with two positive – or two negative – bumps should be classified as a negative sample and a signal with two bumps that have opposite signs should be classified as a positive example. The temporal nature of the signal makes this task non-trivial, as the network of spiking neurons needs to keep track of the first half of the signal in order to make the correct decision. We then trained a spiking network of $N = 384$ neurons to implement the dynamical system described by the RNN. The parameters of the spiking network are given in Table S1.

TABLE S1
PARAMETERS FOR THE TEMPORAL XOR TASK.

Parameter	Value
N_c	1
\hat{N}	64
N	384
τ_{mem}	50 ms
τ_{fast}	–
τ_{slow}	70 ms

Network architectures

We investigated the robustness to simulated noise for four different learning paradigms, including the FORCE method, BPTT and reservoir computing. We implemented FORCE, as well as BPTT using Jax⁵² as part of Rockpool.⁵⁹ To ensure comparability, we chose most of the parameters such as network size and input dimensionality to be the same across different architectures. Table S2 summarises the parameters used for each architecture.

Measurements of parameter mismatch

Using recordings from fabricated mixed-signal neuromorphic chips we measured levels of parameter mismatch (i.e. fixed substrate noise pattern)

TABLE S2
NETWORK ARCHITECTURE PARAMETERS USED DURING NOISE ROBUSTNESS EXPERIMENTS. *: SUBJECT TO MODIFICATION DURING TRAINING.

Parameter	FORCE	BPTT	Reservoir	ADS Network
N_c	16	16	16	16
\hat{N}	128	–	–	128
N	768	768	768	768
τ_{mem}	10 ms	50 ms*	$\mathcal{U}[1e-4, 0.112]$	50 ms
α	0.00001	–	–	–
τ_{syn}	20 ms	70 ms*	$\mathcal{U}[1e-4, 0.112]$	70 ms/1 ms

present in hardware. In particular, for DYNAPTM-SE,² a neuromorphic processor which emulates LIF neurons with alpha and exponential synaptic response using analog circuits, we measured neuron and synaptic time constants and synaptic weights for individual neuron units, by recording and analysing the voltage traces produced by these circuits. We observed levels of mismatch in the order of 10–20% for individual parameters, with parameter spread being proportional to the mean parameter value (see Fig S1).

Measurements were obtained by capturing traces of membrane voltage of individual silicon neuron circuits of the chip using a program controlled oscilloscope. Even though only the neuron membrane voltage could be observed, manipulations of the neuron and synapse circuit biases allow the measurement of various circuit parameters indirectly.

To measure the neuron time constants, neurons were injected with a square step of constant DC current that leads to a stable membrane potential below the spiking threshold (i.e. membrane leakage is equal to constant input current). After the step input is removed the membrane potential voltage decays to resting state, and the resulting trace was fitted with an exponential decay function to extract the membrane time constant for that neuron.

Refractory periods of neurons were measured by injecting the neurons with sufficient constant DC current to emit spikes. Refractory period was measured as the time between the after-spike membrane potential drop until the membrane potential rose back to the 10% level of the overall

trace amplitude.

Synaptic parameters were observed through neuron circuits by setting the neuron time constants to the shortest possible value (i.e. maximizing membrane leakage) so that the membrane voltage directly followed the shape of excitatory and inhibitory synaptic input currents. By stimulating synapses with regular spike trains with low enough rate for the pulses not to interact with each other, the resulting trace amplitude for each pulse amplitude was considered a measure of weight, and the pulse decay time specified the synaptic time constant. Note that the pulse amplitudes should rather be considered as a way of characterizing the relative variability of weights rather their absolute values, as the measurements can only be performed indirectly via the neuron circuit.

RELATIONSHIP BETWEEN ALEMI³⁹ AND FOLLOW³¹ LEARNING RULES

The learning rule proposed in ref. 39 closely matches the FOLLOW³¹ learning rule for the recurrent updates, when a few assumptions are made.

The learning rule described in ref. 39 is given by

$$\dot{\mathbf{W}}^{\text{slow}} = \Psi(r)(\mathbf{D}^T e)^T$$

where $\Psi(r) = \phi(\mathbf{M}r + \theta)$. If we assume $\Psi(r) = r$, which did not have large impact on functionality as demonstrated, we can rewrite the learning rule to

$$\dot{\mathbf{W}}^{\text{slow}} = r(\mathbf{D}^T e)^T$$

The authors use the notation that $W_{i,j}$ is the connection from neuron i to j .³⁹ Since the FOLLOW paper assumes the exact opposite, we rewrite the update rule to

$$\dot{\mathbf{W}}^{\text{slow}} = (\mathbf{D}^T e)r^T$$

We now define the error current as

$$I^\epsilon = \mathbf{D}^T e = \sum_{\alpha=1}^{\hat{N}} D_{\alpha,i} e_\alpha$$

We can now write the update to \mathbf{W}^{slow} as

$$\dot{W}_{i,j} = \sum_{\alpha=1}^{\hat{N}} D_{\alpha,i} e_\alpha (S_j * \kappa) \quad (6)$$

where we replaced r_j with the spike train S_j convolved with the synaptic response kernel κ .

The recurrent update to $W_{i,j}$ in the FOLLOW scheme is given by

$$\dot{W}_{i,j} = (I_i^\epsilon * \kappa^\epsilon)(S_j * \kappa) \quad (7)$$

where $I_i^\epsilon = k \sum_{\alpha=1}^{\hat{N}} D_{i,\alpha}^{\text{FOLLOW}} e_\alpha$

One can see that the updates 6 and 7 are equivalent under the assumptions $\Psi(r) = r$ and $\kappa^\epsilon = \delta$, where δ is the unit impulse kernel.